Color Edge Detection by Photometric Quasi-Invariants

J. van de Weijer   Th. Gevers   J.M. Geusebroek

Intelligent Sensory Information Systems
Faculty of Science, University of Amsterdam
Kruislaan 403, 1098 SJ Amsterdam, The Netherlands
{joostw, gevers, mark }@science.uva.nl

Abstract

Photometric invariance is used in many computer vision applications. The advantage of photometric invariance is the robustness against shadows, shading, and illumination conditions. However, the drawbacks of photometric invariance is the loss of discriminative power and the inherent instabilities caused by the non-linear transformations to compute the invariants.

In this paper, we propose a new class of derivatives which we refer to as photometric quasi-invariants. These quasi-invariants share with full invariants the nice property that they are robust against photometric edges, such as shadows or specular edges. Further, these quasi-invariants do not have the inherent instabilities of full photometric invariants. We will apply these quasi-invariant derivatives in the context of photometric invariant edge detection and classification. Experiments show that the quasi-invariant derivatives are stable and they significantly outperform the full invariant derivatives in discriminative power.

1. Introduction

Photometric invariance is important for many computer vision applications to obtain robustness against shading and illumination conditions. The reflection model by Shafer [7] provides a physical model which allows for the classification of different physical evens, such as shadows and highlights (see e.g. [3]). From this model, several computational methods have been proposed to obtain photometric invariance such as object geometry, camera viewpoint, shadow, shading and specularity invariance [1] [2] [6]. However, the non-linear transformations, often used to compute the photometric invariants, introduce several drawbacks, such as instabilities and loss of discriminative power.

Traditionally, this effect of instabilities is suppressed by ad hoc thresholding of the transformed values. Ohta [5] considers only rgb-values if the intensity is larger than 30 (on a range of 256 values), and rejects hue values if the saturation times the intensity is less than 9. Healey [4] rejects

rgb-values when the RGB-values fall within the sphere of radius 4σ centered at the origin of the RGB space. A more elaborated approach is given by Stokman [8] applying error propagation through the various color spaces to compensate for the undesired effects of the instabilities and nonlinearities of the different photometric invariant spaces. However, the reduced discriminative power due to photometric invariants remains unsolved.

Therefore, in this paper, we propose a new class of derivatives which we refer to as photometric quasi-invariants. This new set is designed according to the following criteria 1. insensitiveness to photometric variation 2. robustness against instabilities, 3. discriminative power. These quasi-invariants are like the full photometric invariants insensitive to shadow/shading/specular edges. However, these quasi-invariants have better discriminative power than the full invariants. Furthermore, they do not have the inherent instabilities of full photometric invariants. Due to the lack of full photometric invariance, the quasi-invariants are unsuited to applications based on comparison of edge responses, such as invariant object recognition. However for a broad domain of applications, such as shadow/shading/specular invariant edge detection, edge classification, and shadow edge insensitive snakes, they are well suited. In this paper, we will apply these quasi-invariant derivatives in the context of photometric invariant edge detection and classification.

This paper is organized as follows. In section 2, the dichromatic reflection model and its first-order derivative are analyzed. A set of photometric variants and quasi-invariants is proposed in section 3. In section 4, experiments are given. Section 5 finishes with concluding remarks.

2. The Dichromatic Reflection Model

In this section the dichromatic reflection model introduced by Shafer [7] is discussed first. From this model, the new set of photometric variants and quasi-invariants is constructed.

The dichromatic model divides the reflection in the interface (specular) and body (diffuse) reflection component

<center>1</center>

for optically inhomogeneous materials. Assuming white illumination (i.e. smooth spectrum of nearly equal energy at all wavelengths) and neutral interface reflection (i.e. the color of the highlight is independent of the wavelength), the RGB vector, $\mathbf{F} = (R, G, B)^T$, can be seen as a weighted summation of two vectors,

$$\mathbf{F} = e(m^b \hat{\mathbf{C}}^b + m^i \hat{\mathbf{C}}^i) \qquad (1)$$

in which $\hat{\mathbf{C}}^b$ is the color of the body reflectance, $\hat{\mathbf{C}}^i$ the color of the interface reflectance (i.e. specularities or highlights), m^b and m^i are scalars representing the corresponding magnitudes of reflection and e is the intensity of the light source. Note that vectors are indicated in bold and the hat is used to denote the unit vector. For matte surfaces there is no interface reflection and the model further simplifies to

$$\mathbf{F} = e m^b \hat{\mathbf{C}}^b \qquad (2)$$

which is the well-known Lambertian reflection. For more on the validity of the photometric assumptions see [1] [7].

Then the spatial derivative of the dichromatic reflection model of eq. 1 is as follows:

$$\mathbf{F}_x = e m^b \hat{\mathbf{C}}^b_x + \left(e_x m^b + e m^b_x \right) \hat{\mathbf{C}}^b + \left(e m^i_x + e_x m^i \right) \hat{\mathbf{C}}^i. \qquad (3)$$

As we assume white illumination and neutral interface reflection, $\hat{\mathbf{C}}^i$ is independent of x. The subscript is used to indicate the spatial derivative. The spatial derivative in eq. 3 is a summation of three weighted vectors, successively caused by object reflectance, shading-shadow and specular change. In this paper, we assume that a shadow is not colored (i.e. assuming that the light in the shadow has the same spectral characteristics as the light in the non-shadow area).

In fact, the direction of the shadow-shading changes (fig.1a) follows from eq. 2. In the absence of interface reflection, the direction of $\hat{\mathbf{C}}^b$ coincides with the direction of $\hat{\mathbf{F}} = \frac{1}{\sqrt{R^2+G^2+B^2}} (R, G, B)^T$. The shadow-shading direction is the multiplication of two scalars denoting two different physical phenomena. $e_x m^b$ indicates a change in intensity which is a shadow edge. And $e m^b_x$ is a change in the geometry coefficient which is a shading edge.

The second direction is the specular direction $\hat{\mathbf{C}}^i$ in which changes of the specular geometry coefficient m^i_x occur. It is equal to $\frac{1}{\sqrt{3}}(1, 1, 1)^T$ since we assume a white light source and neutral interface reflection (fig.1b). The specular direction is multiplied by two factors. Firstly, $e m^i_x$ is a change of geometric coefficient caused by changes in the angles between viewpoint, object and light source. Secondly, the term $e_x m^i$ representing a shadow edge on top of a specular reflection.

Having the direction of two of the causes of an edge, we are able to construct a third direction which is perpendicular to these two vectors (fig.1c). This direction, named body

edge	$\mathbf{S}_x$	$\mathbf{S}^c_x$	$\mathbf{O}_x$	$\mathbf{O}^c_x$	$\mathbf{H}_x$	$\mathbf{H}^c_x$
object	x	x	x	x	x	x
shading	x	-	x	x	x	-
specular	x	x	x	-	x	-

Table 1: The response of the photometric variants and the quasi-invariants to different photometric edges. '+' indicates a response, '-' indicates no response.

direction $\hat{\mathbf{B}}$, is computed by the outer product:

$$\hat{\mathbf{B}} = \frac{\hat{\mathbf{F}} \times \hat{\mathbf{C}}^i}{\left| \hat{\mathbf{F}} \times \hat{\mathbf{C}}^i \right|}. \qquad (4)$$

In the special case of a shadow-shading direction coinciding with the light source direction (i.e. black-white axis), the outer product is undefined. For these points we consider the body direction to be the zero vector $\hat{\mathbf{B}} = \mathbf{0}$. Note that the object direction is *not* equal to the direction in which changes of the object reflectance occur, $\hat{\mathbf{C}}^b_x$. It is perpendicular to the two other causes of an edge. Hence changes in the body direction can only be attributed to an object reflectance change.

In conclusion, changes in the reflection manifest themselves as edges in the image. There are three causes for an edge in an image: an object change, a shadow-shading edge or a specular change. We indicated three directions: the shadow-shading direction, the specular direction and the body direction. This information is used in the next section to construct a set of photometric variants and quasi-invariants.

3. Photometric Variants and Quasi-Invariants

In this section, the goal is to propose a new set of photometric variants and quasi-invariants. To this end, the derivative of an image, $\mathbf{F}_x = (R_x, G_x, B_x)^T$, is projected on three directions found in the previous section. We will call these projections *variants*. E.g. the projection of the derivative on the shadow-shading direction results in the shadow-shading variant. By removing the variance from the derivative of the image, we construct a complementary set of derivatives which we will call *quasi-invariants*. These quasi-invariants are not invariant with respect to a photometric variable. However, they share the nice property with normal invariants that they are insensitive for certain edges, e.g. shadow or specular edges.

The projection of the derivative on the shadow-shading direction is called the shadow-shading variant and is defined as

$$\mathbf{S}_x = \mathbf{F}_x \cdot \hat{\mathbf{F}} \, \hat{\mathbf{F}}. \qquad (5)$$
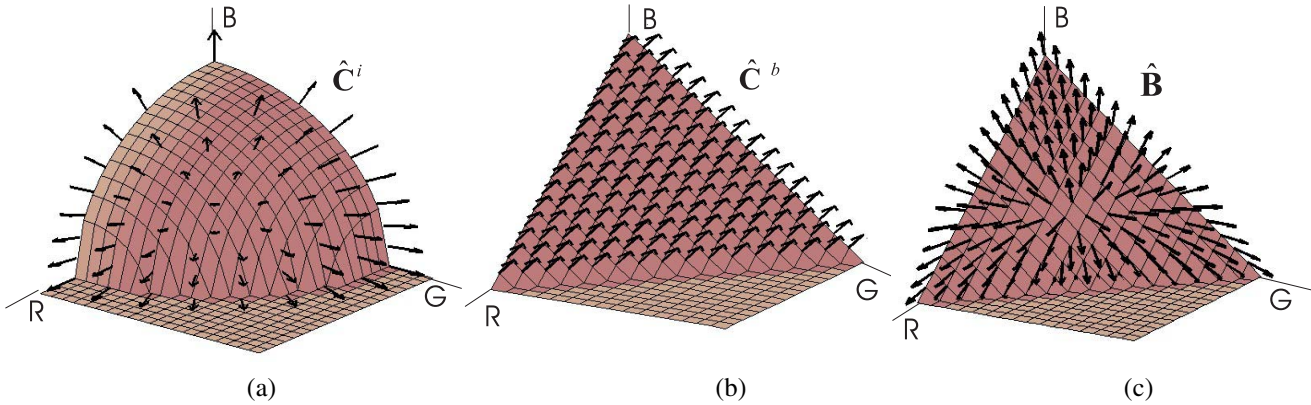
2

IEEE
COMPUTER
SOCIETY

Figure 1: a) The shadow-shading direction. b) The specular direction c) The body direction. For a), and b) the arrows are perpendicular to the depicted planes. For c) the arrows are tangent to the depicted plane.

The dot indicates the vector inner product. The second $\hat{\mathbf{F}}$ gives the direction of the variant. The shadow-shading variant can be interpreted as the part of the derivative which could be explained by a change in the shadow or shading component of the reflectance. Due to correlation of the object and specular direction with the shadow-shading direction, part of $\mathbf{S}_x$ might be caused by changes in object or specular reflection.

Now that we know what the derivative energy in the shadow-shading direction is, we may derive the derivative which remains after substraction of the variant. We call this the shadow-shading quasi-invariant, and indicate it by a superscript c.

$$\mathbf{S}_x^c = \mathbf{F}_x - \mathbf{S}_x \qquad (6)$$

The quasi-invariant has a stronger meaning than the variant. It consists of that part of the derivative which is *not* caused by shadow-shading edges (fig.2b). Hence, $\mathbf{S}_x^c$ does only contain specular, or body edges.

The same reasoning can be applied to the specular direction and results in the specular variant and the specular quasi-invariant

$$\begin{aligned} \mathbf{O}_x &= \mathbf{F}_x \cdot \hat{\mathbf{C}}^i \, \hat{\mathbf{C}}^i \,, \\ \mathbf{O}_x^c &= \mathbf{F}_x - \mathbf{O}_x. \end{aligned} \qquad (7)$$

The specular quasi-invariant is insensitive to highlight edges (fig.2c).

In some cases one might be interested in the part of the derivative which can be explained by either a shadow-shading or a specular change. For this purpose the shadow-shading-specular variant and quasi-invariant are proposed.

$$\begin{aligned} \mathbf{H}_x^c &= \mathbf{F}_x \cdot \hat{\mathbf{B}} \, \hat{\mathbf{B}} \,, \\ \mathbf{H}_x &= \mathbf{F}_x - \mathbf{H}_x^c. \end{aligned} \qquad (8)$$

This quasi-invariant represents the derivative energy in the body direction (see section 2) which is perpendicular to the

shadow-shading and the specular direction. Therefor, $\mathbf{H}_x^c$ does not contain specular or shadow-shading edges (fig.2d). A overview of the photometric variants and quasi-invariants is given in table 1.

3.1. Limitations of Photometric Quasi-Invariants with respect to Classical Photometric Invariants

We introduced a new set of edge detectors, namely the photometric variants and quasi-invariants. Here the difference between the classical photometric invariants (e.g. normalized RGB, hue) and the quasi-invariants is discussed.

The classical invariants are invariant with respect to a photometric parameter like for instance the geometric coefficient m^b in the case of normalized RGB. Hence, the first order derivative response of such invariants does not contain any shadow-shading variation. Our approach determines the direction in the RGB-cube in which shadow-shading edges exhibit themselves. The derivative caused by other than shadow-shading edges can than be computed. Hereby sharing with classical invariants the property that shadow-shading edges are ignored. However, this quasi-invariant is not invariant with respect to m_b.

In the case of the shadow-shading quasi-invariant subtraction from eq. 3 of the part in the shadow-shading direction $\mathbf{C}^b$ results in

$$\mathbf{F}_x = em^b \left(\mathbf{C}_x^b - \mathbf{C}_x^b \cdot \hat{\mathbf{C}}^b \right) \qquad (9)$$

which is clearly not invariant for m^b and e. In a similar way also the specular-shadow-shading quasi-invariant can be proven to be dependent on m^b and e.

This dependency of the quasi-invariants on m^b and e limits the applicability of the filters. The filter can be used to remove the undesired photometric edges. Possible applications are: shadow-edge insensitive snakes, shadow-shading-
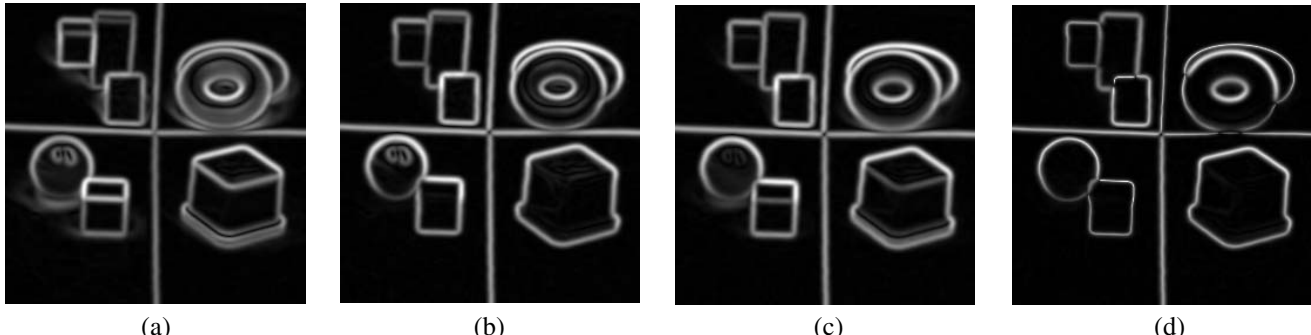
3

Figure 2: Derivatives applied to fig.4a; a) color gradient $\mathbf{F}_x$. b) shadow-shading quasi-invariant, $\mathbf{S}_x^c$. c) the specular quasi-invariant $\mathbf{O}_x^c$. d) the specular-shadow-shading quasi-invariant $\mathbf{H}_x^c$.

specular edge independent corner detection and edge classification. However they cannot be used for applications where edge responses are compared under different circumstances, such as invariant image retrieval.

The specular quasi-invariant is actually the derivative of the well-known opponent color space [8]. After subtraction of the variant direction, the derivative in the plane perpendicular to the $\mathbf{C}^i$ remains. This is equal to the derivative which is acquired in the opponent color space model. It can easily be checked that after substraction of the specular variant from eq. 3 the result is independent of m^i. however, m_i itself is not a physical parameter, it is composed of several physical variables, such as surface patch normal and direction of illumination, which are also represented in m_b. None of the physical parameters disappears from the equation and hence $\mathbf{O}_x^i$ is a quasi-invariant.

4. Experiments

In the introduction we indicated that the classical photometric invariants have limited applicability due to loss of discriminative power and instabilities. Here we will investigate the performance of the quasi-invariants on these two points; 1. stability, 2. discriminative power.

Since the specular quasi-invariant is well-known, its performance is not investigated here (see section 3.1). Both for instability and discriminative power results are compared with photometric invariants. The experiments were performed with rgb, $c_1c_2c_3$, $l_1l_2l_3$, Hue, Cw, Hw [1] [2]. Because the results for these invariants were similar, we chosen normalized RGB and hue as exemplary for the set of invariants, and compared them with the quasi-invariants.

4.1. The Applied Derivatives

The computation of the variants and quasi-invariants is achieved by applying Gaussian kernels. The normalized

RGB is computed with

$$ r = \frac{R}{R + G + B}. \tag{10} $$

For g, b similar equation hold. The edges are computed with

$$ r_x = \frac{R_x \left(B + G \right) - R \left(B_x + G_x \right)}{\left(R^2 + G^2 + B^2 \right)} \tag{11} $$

The hue and its derivative are given by

$$ hue = \arctan \left(\frac{\sqrt{3}(R-G)}{R+G-2B} \right), $$
$$ hue_x = \frac{\sqrt{3}((G-B)R_x + (B-R)G_x + (R-G)B_x)}{2(R^2+G^2+B^2-GR-BR-GB)}. \tag{12} $$

The derivatives $|\mathbf{S}_x|$ and $|\mathbf{H}_{\mathbf{x}}^c|$ follow from eq.5 and eq .8

$$ |\mathbf{S}_x| = \frac{R_x R + G_x G + B_x B}{\sqrt{R^2+G^2+B^2}}, $$
$$ |\mathbf{H}_x^c| = \frac{(G-B)R_x + (B-R)G_x + (R-G)B_x}{\sqrt{2(B^2+G^2+R^2-RG-RB-GB)}}. \tag{13} $$

The quasi-invariant $|\mathbf{S}_x^c|$ follows from the fact that the quasi-invariant and the variant energy sum up to the total derivative energy, $|\mathbf{F}_x|^2 = |\mathbf{S}_x|^2 + |\mathbf{S}_x^c|^2$.

4.2. Instabilities

Photometric invariants inherently have instable points in the RGB-cube. The shadow-shading invariants are unstable for low intensities. Thus little changes around the black-point result in large changes in the invariant plane. This is particularly inconvenient because shadow-shading edges tent to produce low-intensity areas. For the specular-shadow-shading invariants the instability is situated on the black-white axis in the RGB-cube. On this axis the hue is undefined and hence little changes result in large differences between the color-angles.

The photometric quasi-invariants are interpretable as projections in the RGB-cube and remain stable throughout the RGB-cube. In fig.3a a synthetic image of a red-blue
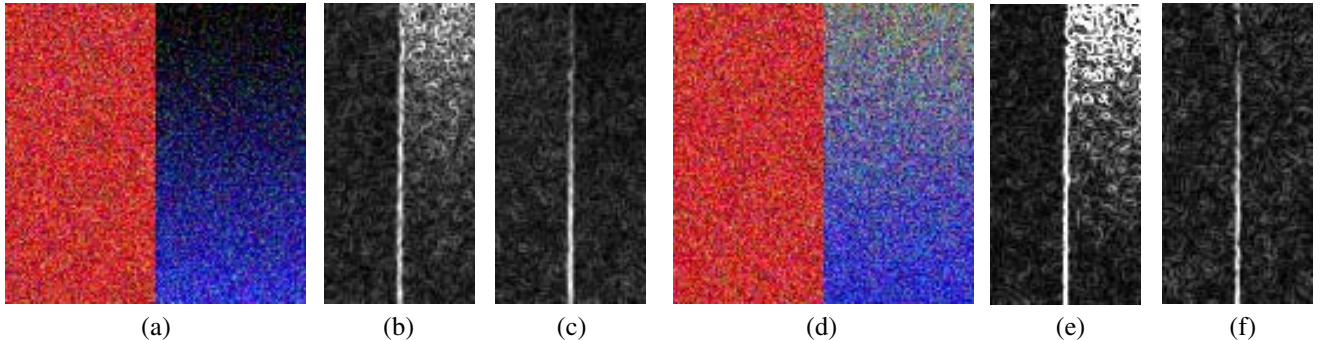
4

Figure 3: a) Red-blue edge, with a decreasing intensity of the blue patch going in the upward direction. b) the normalized RGB derivative. c) The shadow-shading quasi-invariant. d) Red-blue edge, with increasing saturation going in the upward direction. e). the classical hue derivative. f) The specular-shadow-shading quasi-invariant.

edge is depicted. The blue intensity decreases along the y-axis. Gaussian uncorrelated noise has been added to the channels. In fig.3b the normalized RGB response is depicted and the instability for low intensities is clearly visible. For the shadow-shading quasi-invariant (fig.3c) no instability occurs and the response just diminishes for low intensities.

For the hue a similar reasoning holds. In fig.3d a red-blue edge is depicted. The blue patch becomes achromatic with increasing y. The instability is clearly visible in fig.3e whereas in fig.3f the response remains stable.

4.3. Discriminative Power

Here we compare the edge detection performance of the quasi-invariants with the invariants from literature. These results can also be seen as an indication of the loss of discrimination due to invariance. Edge detection is performed between the 1012 different colors from the PANTONE [9] color system. The patches from PANTONE are reduced to one RGB-value by a large Gaussian averaging operation. Every one of the 1012 different RGB-values is combined with all other RGB-values, resulting in a total of $N = 1012 * 1011/2 = 511566$ edges of $M = 25$ pixels length. The edge position is determined by computing the maximum response path of the derivative energy in a region of 20 pixels around the actual edge. This results in an edge estimation which is compared with the actual edge. We define two error measures. First, the average pixel displacement Δ,

$$\Delta = \frac{\sum\limits_{\{x_{i,j}; |x_{i,j} - x_0| > 0.5\}} |x_{i,j} - x_0|}{N \cdot M} \qquad (14)$$

in which $x_{i,j}$ is j-th edge pixel of the i-th edge. Because the actual edge is located between two pixels displacements equal to .5 pixels are considered as a perfect match. Secondly, the percentage of missed edges, ε, is computed. An

std. noise →	5		20	
detector ↓	Δ	ε	Δ	ε
S_x^c	0.043	0.99%	0.43	10%
rgb	0.21	2.0%	1.1	18%
H_x^c	0.35	5.8%	0.98	20%
hue	0.85	9.8%	2.1	34%
$RGB - gradient$	0.003	.07%	0.08	2.0%

Table 2: The displacement, Δ, and the percentage of missed edges, ε, for five different edge detectors. The experiment was conducted with additive Gaussian noise of standard deviation 5, and 20.

edge was classified missed as the variation over one edge,

$$\mathrm{var}(i) = \frac{1}{M} \sum_{j=1}^{M} \left| x_{i,j} - \frac{1}{M} \sum_k x_{i,k} \right| \qquad (15)$$

is larger than 1 pixel. For the Gaussian scale $\sigma = 1$ is chosen. The experiments were performed on the edge dataset after pollution with uncorrelated Gaussian noise of standard deviation 5, and 20.

Uncorrelated Gaussian noise with a standard deviation of 5 and 20 was added to the edges images.

The results are depicted in table 2. For both cases, the shadow-shading and specular-shadow-shading edges, the quasi-invariants substantially outperform the invariants. For many applications for which invariance is desired but impractical due to the loss of discriminative power and inherent instabilities, the quasi-invariants might be the solution.

4.4. Edge Classification

In this experiment edges are classified as being either shadow-shading, specular, or object edge. The photometric variants and quasi-invariants form a good framework for
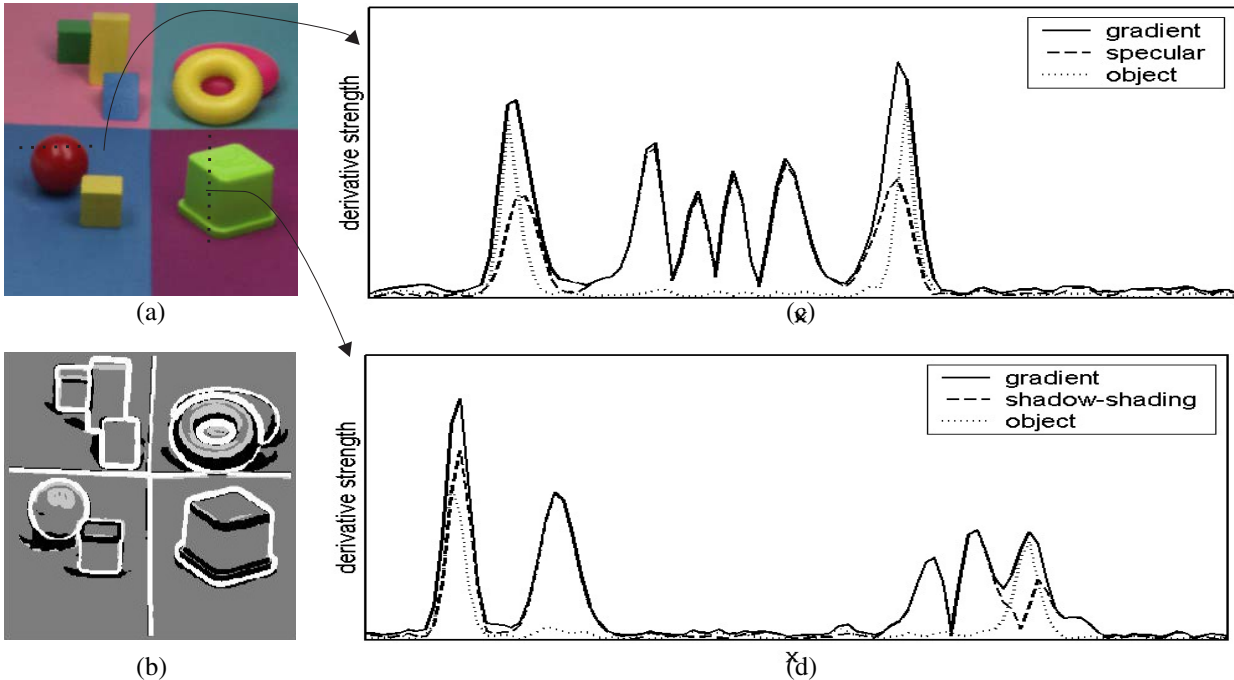
5

Figure 4: a) input image with superimposed two dotted lines which are plotted in the images c and d. b) Edge classification result, with white object edges, black shadow edges and light grey specular edges. c) The derivative strength of the gradient the specular variant and the specular-shadow-shading quasi-invariant (object). d) Derivative strength along a line of the gradient, the shadow-shading variant and the specular-shadow-shading quasi-invariant (object).

such a classification. Primarily because of the conservation of the RGB-cube metric which allows for a quantitative comparison between the different responses. Note that this is not possible for derivatives based on invariants. The normalized RGB derivative can only be compared qualitatively with the hue derivative.

In fig.4 the 'toys' image is shown. Responses along two lines in the image are enlarged in fig.4c and d. The line in fig.4c crosses two object edges and several specular edges. It nicely shows that the specular-variant almost perfectly follows the total derivative energy for the specular edges in the middle of the line. In fig.4d a line is depicted which crosses two object edges and three shadow-shading edges. Again the shadow-shading variant follows the gradient for the three shading edges.

A simple classification scheme results in 4b, in which white indicates object edges, black are shadow-shading edges, and light-grey indicates the specular edges.

5. Conclusions

In this paper, we have proposed a set of quasi-invariant derivatives. Like classical invariants, they are insensitive to certain photometric variation, such as shadow/shading/specular edges. Experiments show that they significantly outperform the full invariants on both

stability and discriminative power. This makes the quasi-invariants well suited especially for edge detection in images of low quality and with poor illumination often encountered in images of snap shot quality as it appears in home video and consumer digital photography in general.

References

[1] J. M. Geusebroek, R. van den Boomgaard, A. W. M. Smeulders, and H. Geerts. Color invariance. *IEEE Trans. Pattern Anal. Machine Intell.*, 23(12):1338–1350, 2001.

[2] T. Gevers and A. Smeulders. Color based object recognition. *Pattern Recognition*, 32:453–464, March 1999.

[3] G.J.Klinker and S.A. Shafer. A physical approach to color image understanding. *Int. Journal of Computer Vision*, 4:7–38, 1990.

[4] G. Healey. Segmenting images using normalized color. *IEEE Transactions on Syst., Man, Cybern.*, 22:64–73, 1992.

[5] Y. Ohta, T. Kanade, and T. Sakai. Color information for region segmentation. *Computer Graphics and Image Processing*, 13:222–241, 1980.

[6] J. Rubin and W. Richards. Color vision and image intensities: When are changes material. *Biological Cybernetics*, 45:215–225, 1982.

[7] S. A. Shafer. Using color to seperate reflection components. *COLOR research and application*, 10(4):210–218, Winter 1985.

[8] H.M.G. Stokman and Th. Gevers. Automatic thresholding and classification of color edges. *Journal of Electronic Imaging*, January 2000.

[9] Paris France. Pantone is a trademeark of Pantone inc. The PANTONE edition 1992-1993, Groupe BASF.

6